

Influence of Electrodeposition Conditions on the Microstructure and Hardness of Ni-B/SiC Nanocomposite Coatings

Weiwei Zhang^{1,*}, Baosong Li^{2,*}

¹ College of Mechanical and Electrical Engineering, Hohai University, Changzhou 213022, China

² College of Mechanics and Materials, Hohai University, Nanjing 211100, China

*E-mail: zdzdq@126.com, bsli@hhu.edu.cn

Received: 10 December 2017 / Accepted: 28 January 2018 / Published: 6 March 2018

In this study, Ni-B/SiC nanocomposite coating was prepared by electrodeposition using trimethylamine borane (TMAB) as boron source in a Ni-B electrolyte containing dispersed SiC nanoparticles. The effects of trimethylamine borane, SiC nanoparticles, current density, thermal treatment on the properties of the electrodeposited coatings were examined by SEM, EDS, XRD et al. The results show that the Ni-B/SiC composite coating exhibits nodular and uniform structure with a desirable interface between the coating and substrate. The as-deposited coatings exhibit Ni (111), Ni (220) and Ni (311) reflections. The boron content in the coating is determined by the ratio of the rate of nickel reduction and the rate of trimethylamine borane decomposition, which facilitates the formation of the amorphous phase. SiC content in the coating can substantially improve the hardness of the coatings under the as-deposited conditions, which promotes the grain refinement due to the fact that particles can act as nucleation sites during the deposition process. Both the boron and SiC nanoparticle content in the deposited Ni-B/ SiC coating decreases as the current density increased from 1 to 7 A dm⁻².

Keywords: Electrodeposition; Ni-B/SiC nanocomposite coating; wear resistance; corrosion resistance; microhardness

1. INTRODUCTION

Composite coatings, which are prepared by incorporation of hard second-phase particles into a metal or alloy matrix, are frequently used to improve the performance of the materials, due to their superior properties such as excellent wear resistance, good corrosion resistance, high hardness and thermal stability [1-3]. If a certain quantity of hard particles are embedded into the matrix phase, the hardness and the wear resistance are expected to be improved largely [4, 5]. Ni-based coatings

reinforced by ceramic particles like Al_2O_3 , TiN, CeO_2 , diamond, SiC, and WC are typical composite coatings which are predominantly employed in industrial applications, especially as a replacement for hard chromium coatings [6]. Among these Ni-based materials, Ni-B coatings are promising due to their advantages of high hardness and superior mechanical wear resistance [7]. During the electro-co-deposition process, the reinforcing particles such as Al_2O_3 [8], TiO_2 [9], SiO_2 [10], diamond [7], SiC [11], CNT [12], MoS_2 [13] and Si_3N_4 [14], which suspended in the electrolyte, are entrapped and embedded in the growing Ni-B matrix either by electrophoresis, mechanical entrapment or adsorption phenomena [15, 16]. Since it combines the advantages of both Ni-B matrix and the reinforcing particles, the Ni-B composite coatings have properties superior to the Ni-B alloys [17, 18]. SiC nanoparticles are broadly used as second-phase reinforcing particles in the composite coating to produce the hard and wear resistant coating due to their good thermal stability, high hardness, wear resistance, commercially available, inexpensive and oxidation resistant [19]. Hence, it can be expected that the SiC nanoparticles could substantially enhance the properties of Ni-B coating, including its mechanical, tribological and anti-corrosion behavior. Ogihara et al. [20] demonstrated that Ni-B/SiC composite coatings could be electrodeposited in conventional Ni electrolyte containing trimethylamine borane as boron precursor. The composite coatings showed superior mechanical properties to Ni/SiC and Ni-P/SiC composite coating. Georgiza et al. [21] reported that incorporation of SiC in Ni-B alloy was obtained in the presence of surfactant tween 20 by electroless plating. It was found that the hardness of the coating was greatly increased and the embedded SiC particles reduce the metallic area prone to corrosion. Krishnaveni et al. [22] reported that dimethylamine borane could also be adopted as a boron source in the electrodeposition of Ni-B films. Bekish et al. [23] examined the relationship between corrosion resistance and structure of electrodeposited Ni-B films and concluded that the corrosion resistance of the nanocrystalline Ni-B coatings is essentially higher than that of the amorphous ones. They clarified that the Ni-B coatings with a relatively low boron content (4 at.%) demonstrate a maximal corrosion resistance. However, till now, Ni-B/SiC [20] composite coatings prepared by electrodeposition have rarely been reported in detail [24]. The co-deposition mechanism of the suspended inert SiC particles into Ni-B matrix has seldom been reported conformably and is still not understood thoroughly [25]. Furthermore, owing to the poor dispersion stability of SiC particles in the plating bath and the low content of SiC in matrix metals, the homogeneous dispersion of SiC particles in the electrolyte is still a key issue to solve.

It is obvious that the development of new Ni-B composite coatings can obtain more excellent properties that well suited to a range of applications. In the present study, we reported on the electro-co-deposition of Ni-B/SiC composite coatings by a conventional electrodeposition technique ensuring that the particle agglomeration is prohibited by the utilization of suitable surfactants and continuous stirring during deposition. The main objective was to elucidate how the microstructure and hardness of the electrodeposited Ni-B/SiC composite coatings depend on the bath composition and deposition parameters, including trimethylamine borane concentration, SiC particles concentration, current density and deposition time.

2. EXPERIMENTAL

Ni-B/SiC composite coatings were prepared by a constant-current electrodeposition method from a typical Watt's Ni bath containing trimethylamine borane as boron source. The bath composition and operating parameters are listed in Table 1. Analytical reagents and deionized water were used to prepare the plating solution. Besides the Ni-B/SiC coating, the Ni-B, Ni/SiC coatings were also prepared for comparison using this bath only without SiC particles or TMAB, respectively. The Cu substrates were masked with insulated tapes to leave 20×20 mm² of exposed area. A nickel plate was used as counter electrode. The Cu and Ni plates were positioned vertically in a 200 ml electrodeposition baths. The distance between the Cu and Ni was fixed around 25 mm. The average size of the as-received SiC particles (purity >99.9%) was ≤150 nm. The electrolytes were stirred for 24 h just before electrodeposition to obtain de-agglomerated particles. The electrodeposition current densities were varied from 0.5 to 7 A dm⁻², SiC particles 2.5 to 12.5 g L⁻¹, and TMAB 0 to 9 g L⁻¹. The pH values of the baths were adjusted to 3.5 using H₂SO₄ or NiCO₃. The resulting coatings were washed with water and dried in air at room temperature. Thermal treatment was conducted in an electric furnace that had been heated to 200 to 600 °C in air, and kept at that temperature for 1 h.

Table 1. Electrolyte composition and electrodeposition parameters for Ni-B/SiC composite coatings.

Electrolyte composition		Electrodeposition parameters	
NiSO ₄ ·6H ₂ O	200 g/L	pH	3.5 ± 0.1
NiCl ₂ ·6H ₂ O	50 g/L	Temperature	40-45 °C
H ₃ BO ₃	35 g/L	Current density	0.5- 7 A·dm ⁻²
Trimethylamine borane(TMAB)	3 g/L	Agitation rate	450 ± 50 rpm
Sodium dodecyl sulfate(SDS)	0.5 g/L	Electrode distance	2.5 cm
Saccharine	1 g/L	Deposition time	15-90 min
SiC nanoparticles	0-15 g/L	Anode	Ni plates

A scanning electron microscope (SEM, model HITACHI-S3400N) coupled with Oxford INCA energy dispersive X-ray spectroscopy (EDS) was utilized to investigate the surface morphology. Specimens for cross-sectional images were prepared by embedding coatings in epoxy resin and polishing using a polisher. XRD patterns were measured with D8 Advance model diffractometer using a Cu K α radiation at room temperature. The microhardness in the cross-regions or surface of the coatings was measured using a Vickers's microhardness indenter with a load of 50 g for 10 s, and the average value of 5 measurements was reported as the microhardness of the deposits.

3. RESULTS AND DISCUSSION

3.1 Microstructure of the electrodeposited Ni-B/SiC composite coatings

Fig.1 shows the results of the XRD patterns of the Ni-B/SiC coating prepared in the bath containing 3, 6 and 9 g L⁻¹ TMAB, respectively. As shown in Fig. 1, the composite coating exhibits broad Ni (111) peak. Compared to the pure Ni, the most obvious change in XRD patterns of Ni-B/SiC

is the disappearing of sharp Ni (200) peak at 52.0° and the broadening of Ni (111) peak at 42.7° , indicating a series of new amorphous structures were formed which lead to novel physical properties. There are no extra peaks that could be attributed to the presence of the intermetallic phases Ni_3B or Ni_2B [26-28]. The broad Ni (111) peak indicates an amorphous nature of the coating in its as-deposited state. It indicates that there is a direct correlation between the B content in the coating and the amorphous structure growth in the nanocomposites. Thus, it indicates that the incorporation of B in the coating resulted in an amorphous structure of the coatings.

The presence of broad peak in as deposited Ni-B/SiC coating can be further explained that Ni-B coatings are solid solution of boron in fcc Ni lattice. According to literature [23], the peaks of (220) (311) reflections were completely disappeared in the XRD pattern of the amorphous Ni-B alloy. However, compared with Ni-B alloy, in addition to the texture (111) orientation, the peaks of Ni (220) and (311) could also be noticed due to the incorporation of SiC nanoparticle into Ni-B matrix. It demonstrates that the boron content in the coating has the function of grain refinement, and facilitates the formation of amorphous structure. The finer the grain size is, the more amorphous character of the coatings is prevalent. Ni-B deposits form solid solution through B displaces a part of nickel atoms into the nickel crystal lattice. With the increase of B content, Ni content in the deposits decreases which facilitates the formation of amorphous structure. This is well consistent with the previous studies [29, 30].

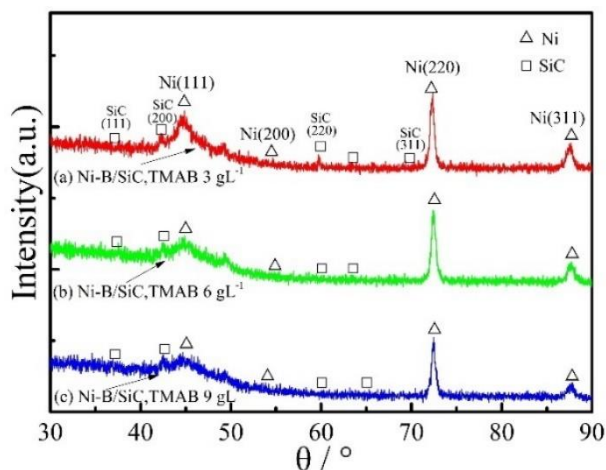


Figure 1. XRD patterns of Ni-B/SiC composite coatings electrodeposited with different TMAB concentration in electrolyte.

Fig.2 shows the XRD patterns of Ni-B/SiC coatings in as-deposited states as a function of SiC particles concentration in the bath. It shows that the formation of the crystalline structure was slightly facilitated with the increase of the particle concentration in the bath. The preferred orientation of electrodeposited coatings is significantly affected by adsorbed species. The preferred orientation of Ni-B films is affected by the adsorption of not only H_{ads} , $\text{Ni}(\text{OH})_2$, H_2 molecules but also boron sources and their decomposition products. Now, the change in the preferred orientation of electrodeposited Ni-B films is still unclear. As hardening element, SiC can improve the hardness of the coating and strengthen the Ni-B matrix which has better wear resistance.

As it is evident, the incorporation of SiC nanoparticles has also resulted in significant grain refinement of the Ni-B matrix. This refinement in grain size is quite desired as the fine grain structure leads to enhanced mechanical properties. The mechanism of grain refinement is that SiC particles which adsorb cations under high potential gradient transported to and then adsorbed on the cathode surface by electrophoresis during the electrodeposition process [31]. Since the incorporated particles decrease the active cathode surface, the electro crystalline potential will increase. In addition, the occurrence of new nuclei in the form of nanoparticles limits the growth of the original crystal grains [32, 33]. Moreover, the incorporation of SiC nanoparticles into the growing Ni-B matrix also improves the corrosion resistance of the deposits due to the decrease of active cathode surface area.

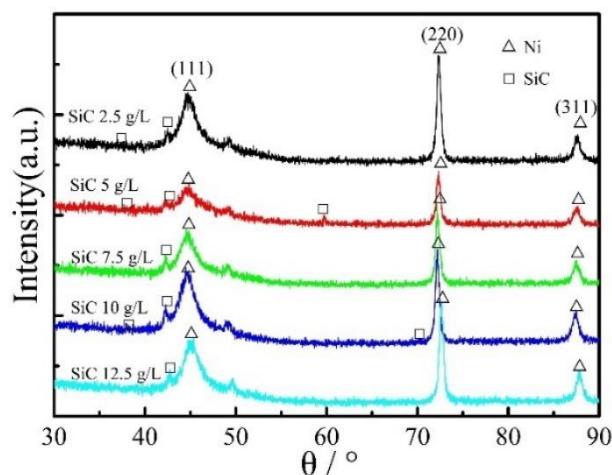


Figure 2. XRD patterns of Ni-B/SiC composite coatings electrodeposited with different SiC particles concentration in electrolyte.

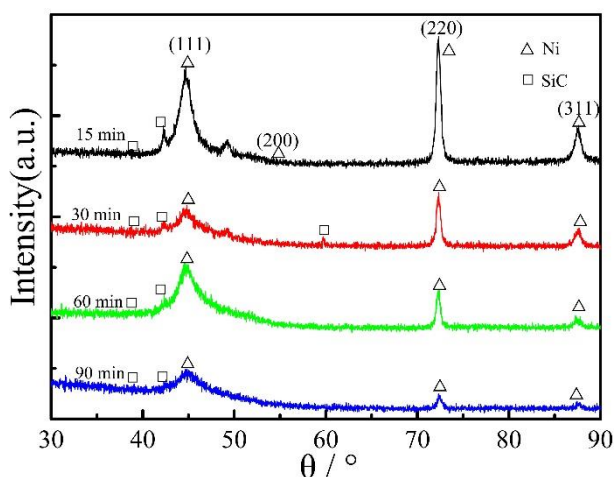


Figure 3. XRD patterns of Ni-B/SiC composite coatings electrodeposited for different time.

Fig. 3 shows XRD patterns of the deposits as a function of deposition time. In general, the intensity of the Ni (111), (220) and (311) reduces with the extension of deposition time. As can be seen in Fig.3, it is apparent that long deposition time facilitates the amorphous structure of the coating.

Meanwhile, the SiC content in the coating decreases when the deposition time exceeds 30 min (see Fig.8). This implies two possible reasons regarding its structural variation. One is the formation of the amorphous Ni-B structure by randomly incorporating B atoms into the FCC lattice of Ni. The other is the growth of small nanocrystallites by incorporation of nanoparticle into the matrix which can be used as nucleation sites. The two structural changes could bring about positive effects on strengthening the composite coatings [34-36].

Fig. 4 displays the XRD patterns of the Ni-B/SiC composite coating electrodeposited at 0.5, 1, 3, 5 and 7 $\text{A}\cdot\text{dm}^{-2}$. The Ni (111), Ni (220) and Ni (311) reflections in the XRD patterns was observed corresponding to the phase angle 44.7° , 72.5° , 87.7° , respectively. As shown in Fig.4, the Ni (220) peak was the main crystal orientation at 0.5 $\text{A}\cdot\text{dm}^{-2}$. With the increase of current density, the broad peak of Ni (111) gradually increased and sharpened. At the same time, the intensity of Ni (220) and Ni (311) decreased, which indicates that the crystal orientation was changed to (111) reflections. When the current density is below 1 $\text{A}\cdot\text{dm}^{-2}$, the existence of the broad peak of Ni (111) shows the coatings are mainly amorphous. In fact, the crystal structure of Ni-B/SiC can be crystalline or amorphous mainly based on the amount of boron and SiC particle content. This result indicated that high current density will change the parent amorphous structure into crystalline and enhances the surface roughness with considerable grain size increasing. The finer of the coating grain is, the more amorphous structure was formed. Therefore, it can be concluded that amorphous structure of the coating is easily obtained at low current density. Crystalline will be promoted at high current density.

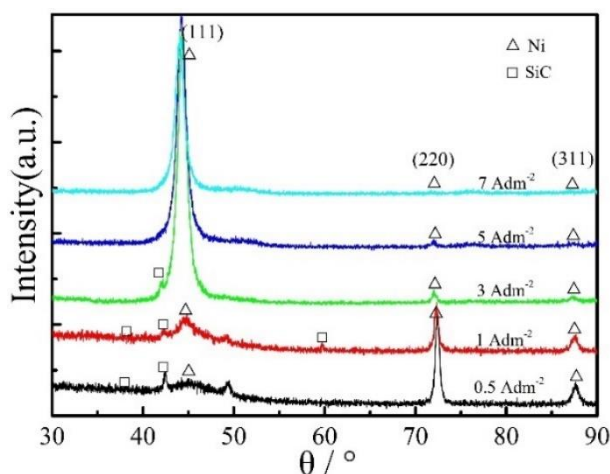


Figure 4. XRD patterns of Ni-B/SiC composite coatings electrodeposited at different current density.

3.2 Morphology and composition of the Ni-B/SiC composite coatings

Fig.5. shows the surface morphology of the as-deposited Ni-B/SiC coating as a function of TMAB concentration in the deposition bath. As shown in Fig.5, obviously, different from the rough and dull surface of the Ni coating consisting of pyramidal crystallites, the surface of Ni-B/SiC coating reveals the formation of nodular, uniform and crack free structure. With the increase of the TMAB concentration, the surface becomes nodular and spherical particles differ widely in size. The size of

spherical particles becomes more uniform when more amorphous structure is formed. However, when TMAB is up to 9 g L^{-1} (Fig.5d), the evenness of the coating decreases with the grain size enlarged. It was reported that the internal stress increases with the increase of boron content in the coatings. These findings are consistent with previous studies [32, 37]. Interestingly, it needs to be pointed out that the coatings prepared without TMAB probably contains some B, below 2 wt.% due to the boric acid in the bath. The mechanism of co-deposition of boron in Ni-B coatings is not yet fully understood. It is supposed that boron is incorporated into Ni-B coating attributing to the adsorption of TMAB on the surface of the formed nickel, which is then decomposed to elemental boron. Therefore, the amount of boron co-deposited with nickel can be determined by the distribution of TMAB, regardless of the electrode potential.

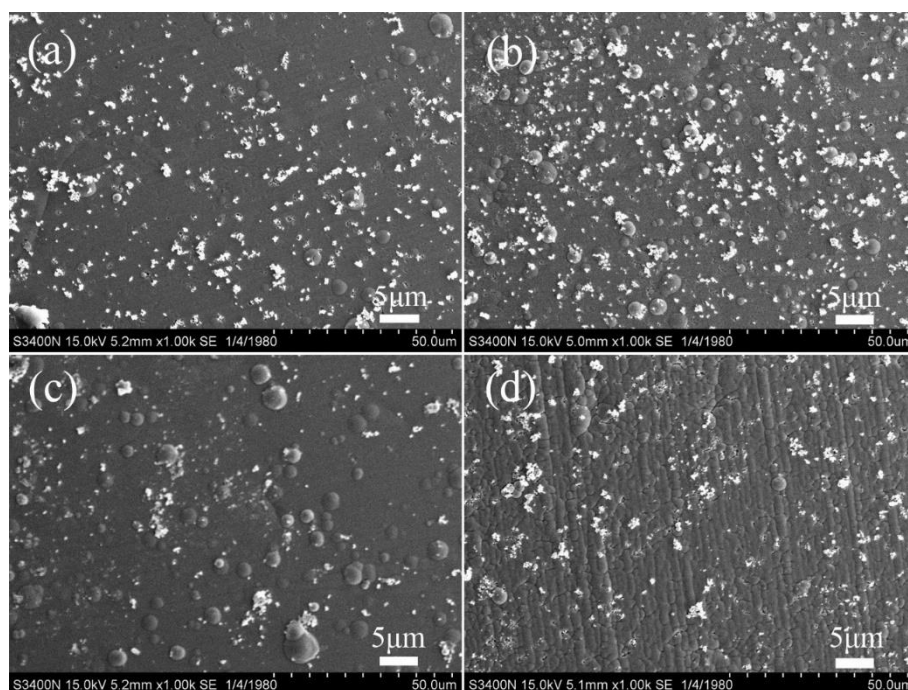


Figure 5. SEM images of electrodeposited Ni-B/SiC composite coatings, TMAB concentration (a) 0 g/L, that is Ni/SiC; (b) 3; (c) 6 and (d) 9 g/L.

Fig.6 is the morphology of the Ni-B/SiC coating deposited at different concentration of SiC nanoparticles. As shown in Fig. 6, the nodular surface of the composite coating was smooth, uniform and fine grained with a few agglomerations on it. During electrodeposition process, SiC particles are incorporated into Ni-B matrix. At constant co-deposition current density ($1 \text{ A} \cdot \text{dm}^{-2}$) and the same deposition time (30 min), there is a moderate drop of SiC content in Ni-B deposited matrix when SiC concentration in the bath is more than 12.5 g L^{-1} . This decreasing trend might be linked to the SiC nanoparticle agglomeration. It suggested that the amount of co-deposited SiC increased with the SiC nanoparticles up to a certain concentration. The preferable concentration of SiC nanoparticles was 5 to 10 g L^{-1} , which would reach a maximum volume percentage of SiC in the Ni-B composite coating. Increasing the concentration of SiC in the electrolyte improves the amount of adsorbed SiC

nanoparticles on the surface of the growing deposit which results in more nanoparticles incorporation in the coating. It is observed that the SiC content in the coatings increases with the increase of SiC concentration in the plating bath from 2.5 to 12.5 g L⁻¹. Meanwhile, the SiC nanoparticles dispersed in the composite coatings increase the number of nickel crystal nucleation and inhibit the growth rate of the already formed nickel crystal grains. The incorporation of SiC nanoparticles into the growing Ni-B matrix results in the decrease of the active cathode surface, which improves the corrosion resistance of Ni-B coating. Nevertheless, when the concentration of SiC surpasses 12.5 g L⁻¹, owing to the adsorption of highly agglomerated particles into the surface, porosity will emerge on the coating which is rarely filled by the deposited Ni ions. The hydrogen generation and high level of particle collision can also promote the porosity generation at the high particle concentrations.

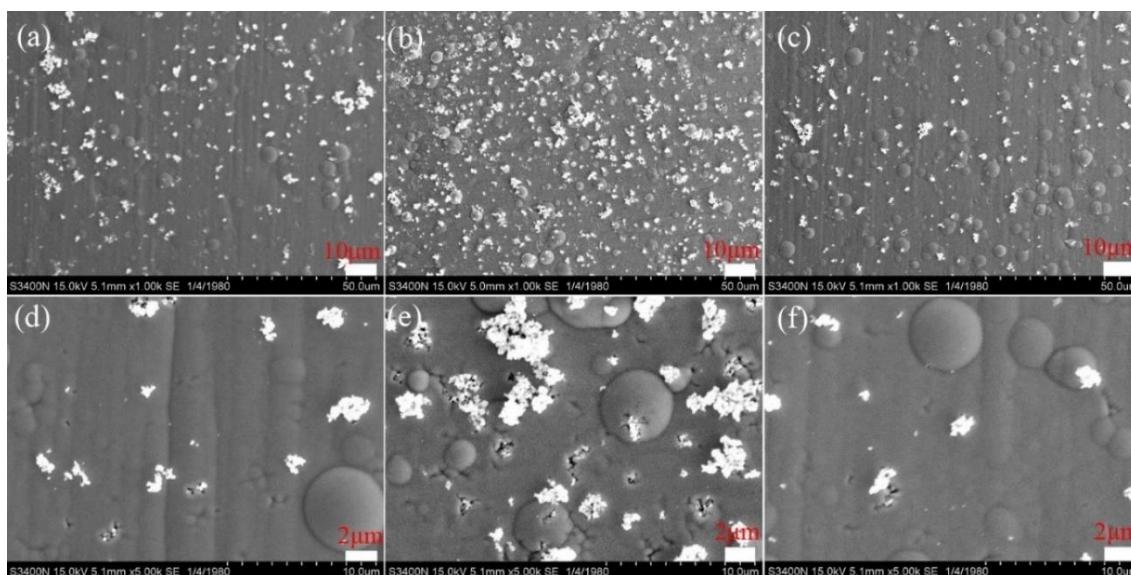


Figure 6. SEM images of electrodeposited Ni-B/SiC composite coatings with SiC concentration in electrolyte (a) 2.5; (b) 5 and (c) 12.5 g/L at low and high magnification.

To show the thickness, interface of the coating, as well as the distribution of SiC particles in the bulk of the coating, the cross-sectional SEM image of the coating was also performed. Fig.7 shows the cross-sectional morphologies of Ni-B/SiC coatings deposited at various current densities for 30 min. It shows that the dark SiC nanoparticles dispersed well into the Ni-B matrix, and few agglomeration phenomena can be observed. As can be seen in Fig.7, the microstructure is compact, and the distribution of the reinforcing SiC particles in the Ni-B matrix is roughly uniform. As it is evident, a desirable interface with no detectable porosity or delamination between the coating and substrate was obtained. The cross-sectional images show that the coating thickness is 6.3, 8.4, 23 and 39.5 μm corresponding to the current density of 0.5, 1, 3 and 5 A·dm⁻², respectively. Then it can be calculated that the deposition rate is 12.6, 16.8, 46 and 79 μm h⁻¹, respectively. In general, the electrodeposition process will be promoted with the increase of current density. The optimal current density of co-deposition is not the highest value because more internal stress will be accumulated due to the intense

hydrogen evolution reaction at high current densities which leads to the formation of microcracks. It is easy to get uniform, dense, fewer cracks and fine-grained coating at 1 to 3 A·dm⁻².

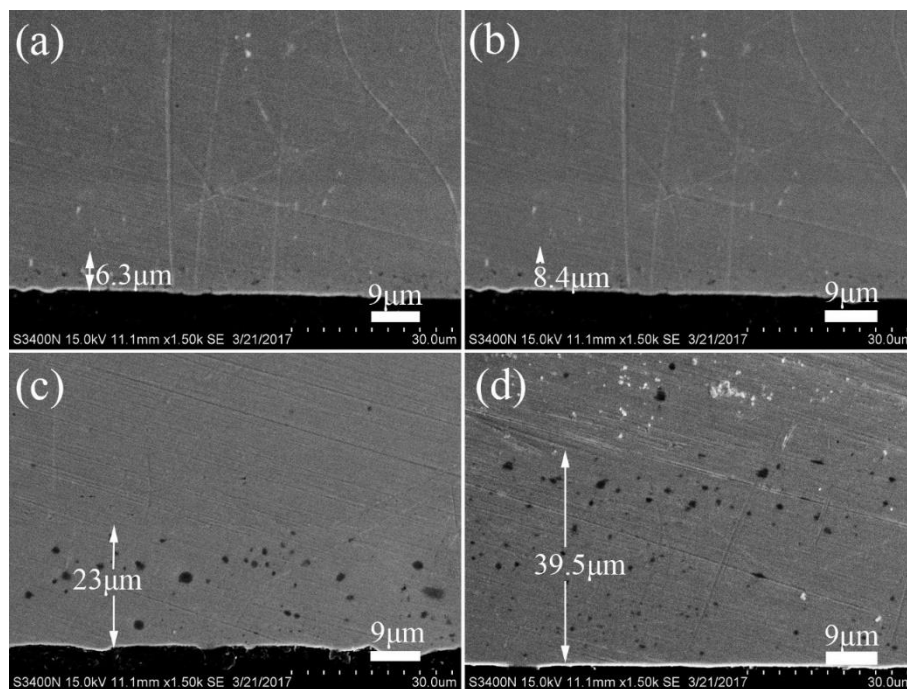


Figure 7. Cross-sectional SEM images of Ni-B/SiC composite coatings electrodeposited at (a) 0.5; (b) 1; (c) 3 and (d) 5 A dm⁻².

The EDS spectrums of the Ni-B/SiC composite coating prepared at different parameter are presented in Fig. 8. As well as Ni peaks, peaks corresponding to B and Si are also visible. That is, the SiC particles were properly incorporated into the Ni-B matrix during deposition. This result suggests that SiC particles can be successfully co-deposited in Ni-B coatings using TMAB as boron source under acidic conditions.

As can be seen in Fig.8 (b, d), increasing the current density from 1.0 to 5.0 A·dm⁻², the SiC content slightly decreased. This is because the co-deposition rate of the SiC particles is almost the same while the deposition rate of Ni increased fast with the increase of current density. The amounts of particles incorporated into the metal matrix are determined by the rate of the particles and cations arrive at the cathode surface. With the increase of current density, the deposition rate of Ni²⁺ ions is faster than the rate of inert particles transfer to the cathode surface. Moreover, the increase in polarization caused by higher current densities results in intensification of hydrogen evolution which will decrease of the incorporated particles [5]. Intense hydrogen evolution process resulted in the formation of large amounts of gas bubbles on the cathode surface, which may hinder the adsorption of SiC nanoparticles on the growing deposit. Fig. 8(b, c) is the EDS spectrum of the Ni-B/SiC coatings deposited for 30 min and 60 min. It shows that the composite coatings contain Ni, B, Si elements, and the SiC nanoparticles were incorporated into the Ni-B matrix. The crystalline structure of Ni-B/SiC

coating is mainly affected by two factors, namely the B content in the Ni-B matrix and the SiC nanoparticle content in the composite coating.

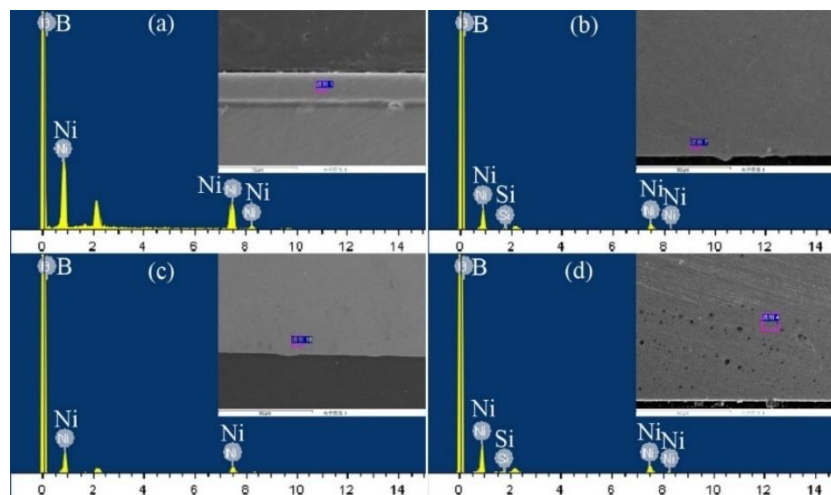


Figure 8. EDS spectra of electrodeposited Ni-B/SiC composite coatings (a) without SiC, 1 A dm^{-2} , 30 min (b) SiC 5 g L^{-1} , 1 A dm^{-2} , 30 min; (c) SiC 5 g L^{-1} , 1 A dm^{-2} , 60 min; (d) SiC 5 g L^{-1} , 5 A dm^{-2} , 30 min.

3.3 Hardness and SiC particle content of the composite coating

Fig. 9 displays the effects of SiC particle concentration in the bath on the hardness and the SiC content in the electrodeposited Ni-B/SiC composite coatings. The hardness of the Ni-B/SiC composite coating was measured before and after thermal treatment at $300 \text{ }^\circ\text{C}$ in air for 1 h. It shows that the microhardness in the as-deposited state increases significantly from 680 HV up to 920 HV with the increase of SiC concentration. However, further increasing SiC to above 10 g L^{-1} led to a slight decrease of the microhardness. Moreover, it was noticed that thermal treatment drastically increased the hardness. It can be seen that the hardness of the coating prepared with 8 g L^{-1} SiC in the bath was improved to 1450 HV after heat-treatment 1 h at $300 \text{ }^\circ\text{C}$. Fig.9 also shows that, initially, the incorporation rate is enhanced and the quantity of the co-deposited SiC particles increases. Then, when SiC concentration exceeds 8 g L^{-1} , the SiC content keep approximately constant. This is because the SiC particles are saturated in the composite coating. That is, the optimum particle concentration in the electrodeposition bath is around 8 g/L . At the higher concentrations of the nanoparticles, a decrease in the deposited particles is evident, which was attributed to the increase of the nanoparticle agglomeration and the enhancement of elastic collisions between the particles. Since the capturing capacity of the growing metal matrix remains virtually constant, a longer period is required for the nanoparticles to be embedded into the Ni matrix by increasing the particle contents in the electrolyte [21, 38].

The strengthening mechanism of composite coatings can be mainly attributed to two factors. One is the amounts of hard particles incorporated into the coatings matrix, which provides the dispersion strengthening effect. The other is the microstructure change of coating matrix which caused

by the embedded second phase. It is well known that appropriate thermal treatments harden Ni-B coating because of the phase transition from amorphous Ni-B alloy to hard Ni₃B and Ni₂B alloys [39]. SiC content promotes dispersion strengthening, increasing mechanical property of the coating. However, SiC nanoparticles will agglomerate when excessive SiC particles were added into the bath and tend to cause porous structure in the grain boundaries. This decreasing trend might be linked to the SiC nanoparticle agglomeration. It will inhibit the effect of dispersion, ultimately lead to a deterioration of the mechanical property.

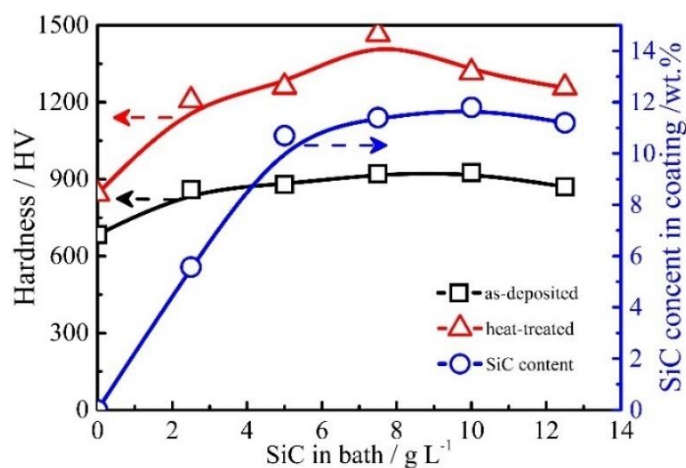


Figure 9. Hardness and SiC content of Ni-B/SiC composite coating as a function of the SiC concentration in the plating bath.

Fig. 10 shows the hardness and boron content of Ni-B/SiC coatings prepared at different current densities. As seen in Fig.10, the hardness of Ni-B/SiC nanocomposite coating reaches the maximum value of 1510 HV when the current density is 1 A·dm⁻². Continue to increase the current density, the hardness gradually decreased to 1214 HV. As for SiC content, with the increase of the current density, the SiC content initially increases, then decreases with the maximal value of 11.76 wt% at 1 A dm⁻². The content of SiC in Ni-B/SiC composite coating remarkably decreases from 11.76 wt.% to 4.05 wt.% by increasing current density from 1 to 7 A·dm⁻². The reason why SiC content depended on current density could be explained as follows. Since the rate of electrodeposition of Ni-B was electron transfer controlled, the growth rate of Ni-B proportionally increased with the current density. However, the co-deposition rate of SiC particles was irrelevant to current density because the co-deposition was initiated by the adsorption of particles on the electrode surface, and then, the adsorbed SiC particles are surrounded with electrodeposited Ni-B. The amounts of particles incorporated into the metal matrix are determined by the rate of the particles and cations arrive at the cathode surface. Thus, it is possible that the SiC content was relatively influenced by current density because only the growth rate of Ni-B was changed by current densities. With the increase of current density, the deposition rate of Ni is faster than the rate of inert SiC particle transfer to the cathode surface. Although this explains the tendency at current densities above 1 A dm⁻², it would not explain the changes in SiC content at current density below 1 A dm⁻². When the current density is below 1 A

dm⁻², the effect of sedimentation and convection on the SiC particles adsorbed on the surface of the growing coating would not be negligible. That is, in a relatively lower current density range, there is an increase in the flux of particles with increasing current density and later a decrease in the higher current density region.

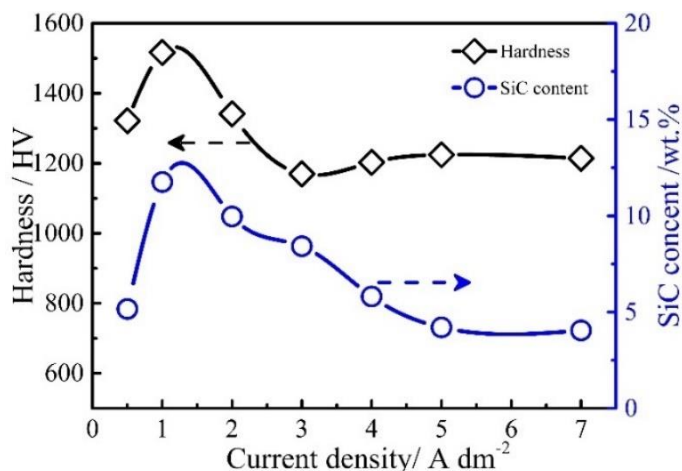


Figure 10. Hardness and SiC content of Ni-B/SiC coating as a function of current density.

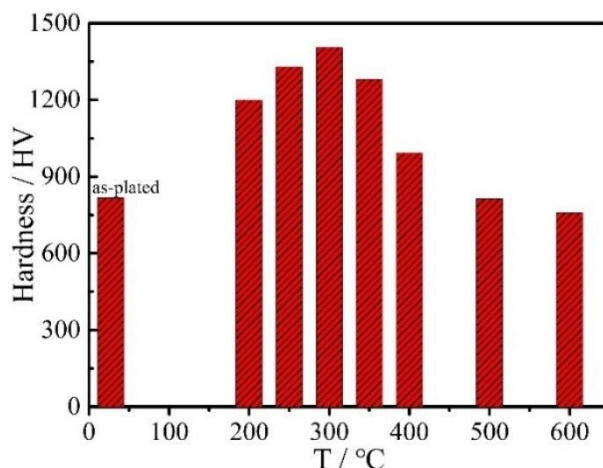


Figure 11. Hardness of Ni-B/SiC coatings as a function of heat-treatment temperature.

The effect of thermal treatment on the hardness of Ni-B/SiC coatings is shown in Fig.11. Compared to the hardness of electrodeposited Ni-B coating in as-deposited states, not much has changed in hardness at the temperatures lower than 200 °C. With further increase in temperatures, the hardness increases rapidly as the structure of the coatings begins to change. As shown in Fig. 11, the hardness of as-deposited Ni-B/SiC coating is 760 HV, and it increases significantly as the treatment of temperature increases, reaching its highest value 1390 HV after heat treatment at 300 °C for 60 min. Then, further increase the temperature results in an obvious decrease in hardness. The obvious increase in hardness was attributed to that higher thermal treatment temperatures favor the precipitation of nickel boride (Ni₃B) and increase the Ni crystal size. When heat treatment temperature is less than or

equal to 300 °C, the increase of grain size is slight. However, beyond 300 °C, the grain size increases considerably and exceeds the size of Ni₃B phase. Then the hardness of the Ni-B/SiC coating was reduced. The formation of hard Ni₃B particles enhances the hardness of the coatings. Owing to excess heat treatments, the grain coarsening decreases the hardness of the coating.

Fig. 12 shows the hardness of Ni-B/SiC coatings as a function of TMAB concentrations in the bath. As shown in Fig.12, the coating hardness was drastically influenced by adding a small amount of TMAB in baths. It was noticed that the hardness increases from 470 HV up to the highest level of 1010 HV with the TMAB concentration up to 2 g L⁻¹. Then, continue to increase the TMAB concentration, the hardness of the composite coating decreased slightly to 930 HV. However, considering the standard deviation, it can be deemed that this hardness value is practically constant. It indicated that co-deposited boron atoms had a beneficial effect on the hardness of the coating. Nevertheless, it was also observed that the coating hardness was stable whereas the boron content increased largely when adding 2 to 10 g L⁻¹ TMAB in the bath. Therefore, it seems that the relationship between coating hardness and boron content is complex. These results indicate that the hardness of the coatings is not only related to the B content in the coating but also the crystalline structure, crystal size, and other factors. The most important effect of the TMAB is the transformation of the crystal structure of Ni to amorphous phase of Ni-B which improves the microhardness. In addition, the proper TMAB has the beneficial effect in grain refinement. More work needs to be done to investigate their influence on the hardness of Ni-B/SiC coatings.

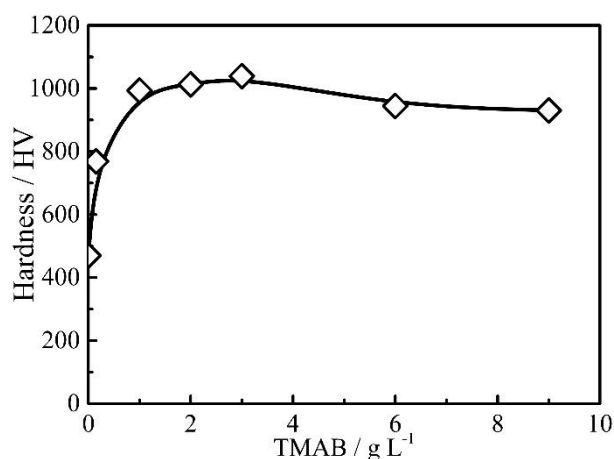


Figure 12. Hardness of Ni-B/SiC coating electrodeposited at 2 A dm⁻² as a function of TMAB concentration in the plating bath.

4. CONCLUSIONS

In this study, Ni-B/SiC composite coating has been fabricated by electrodeposition using TMAB as boron precursor in a Ni-B electrolyte containing suspended SiC nanoparticles. The results indicate that SiC incorporation is achieved using TMAB as boron source, which promotes the grain

refinement due to the fact that nanoparticles can act as nucleation sites during the deposition process. The surface and cross-sectional images show that the Ni-B/SiC composite coating exhibits nodular and uniform structure with a desirable interface between the coating and substrate. XRD patterns of as-deposited coatings exhibit the presence of Ni (111), Ni (220) and Ni (311) reflections, indicating that the nucleation of nickel phase is not completely prevented. Addition of TMAB, SiC nanoparticles led to a significant increase in hardness of the coatings under the as-deposited states as well as after a heat treatment due to the dispersion hardening of the added hard SiC nanoparticles and the grain refinement of Ni-B matrix. The deposition rate increases with the increase of current density whereas the boron content decreases by increasing the current density from 1 to 7 A dm⁻². At high current density, the SiC content relatively decreases because the co-deposition rate of SiC particles was irrelevant to the current density. The co-deposition of SiC was initiated by the adsorption of particles on the electrode surface, while the growth rate of Ni-B proportionally increased with the current density. The boron content in the electrodeposited Ni-B alloy coating is determined by the ratio of the rate of nickel reduction and rate of TMAB decomposition. In principle, we can also modify the hardness of the Ni-B/SiC coating by regulating the current density.

ACKNOWLEDGEMENTS

This work was supported by the National Natural Science Foundation of China (Grant No. 51605137, 51679076)

References

1. F. Madah, C. Dehghanian, A.A. Amadeh, *Surf. Coat. Technol.*, 282 (2015) 6-15.
2. İ. Çelik, M. Karakan, F. Bülbül, *Proc. Inst. Mech. Eng. Part J J. Eng. Tribol.*, 230 (2015) 57-63.
3. B. Li, W. Zhang, W. Zhang, Y. Huan, *J. Alloys Compd.*, 702 (2017) 38-50.
4. M.H. Allahyarzadeh, M. Aliofkhaezai, A.R.S. Rouhaghdam, V. Torabinejad, *J. Alloys Compd.*, 666 (2016) 217-226.
5. D. Ekmekci, F. Bulbul, *Bull. Mater. Sci.*, 38 (2015) 761-768.
6. Y. Liang, Y. Li, Q. Yu, Y. Zhang, W. Zhao, Z. Zeng, *Surf. Coat. Technol.*, 264 (2015) 80-86.
7. O.R. Monteiro, S. Murugesan, V. Khabashesku, *Surf. Coat. Technol.*, 272 (2015) 291-297.
8. W. Sun, P. Zhang, K. Zhao, M. Tian, Y. Wang, *Wear*, 342 (2015) 172-180.
9. S. Huang, Y. Hu, W. Pan, *Surf. Coat. Technol.*, 205 (2011) 3872-3876.
10. S. Sadreddini, A. Afshar, *Appl. Surf. Sci.*, 303 (2014) 125-130.
11. Y. Yao, S. Yao, L. Zhang, *Surf. Rev. Lett.*, 13 (2006) 489-494.
12. C. Guo, Y. Zuo, X. Zhao, J. Zhao, J. Xiong, *Surf. Coat. Technol.*, 202 (2008) 3246-3250.
13. Z. Huang, D. Xiong, *Surf. Coat. Technol.*, 202 (2008) 3208-3214.
14. K. Krishnaveni, T.S.N. Sankara Narayanan, S.K. Seshadri, *J. Alloys Compd.*, 466 (2008) 412-420.
15. F. Cai, C. Jiang, Z. Zhang, V. Ji, *Ceram. Int.*, 40 (2014) 15105-15111.
16. I. Tudela, Y. Zhang, M. Pal, I. Kerr, A.J. Copley, *Surf. Coat. Technol.*, 276 (2015) 89-105.
17. J.L. Wang, R.D. Xu, Y.Z. Zhang, *Trans. Nonferrous Met. Soc. China*, 20 (2010) 839-843.
18. Y.W. Yao, S.W. Yao, L. Zhang, H.Z. Wang, *Mater. Lett.*, 61 (2007) 67-70.
19. M. Ghaderi, M. Rezagholizadeh, A. Heidary, S.M. Monirvaghefi, *Prot. Met. Phys. Chem. Surf.*, 52 (2016) 854-858.
20. H. Ogihara, H. Wang, T. Saji, *Appl. Surf. Sci.*, 296 (2014) 108-113.
21. E. Georgiza, V. Gouda, P. Vassiliou, *Surf. Coat. Technol.*, 325 (2017) 46-51.
22. K. Krishnaveni, T.S.N. Sankara Narayanan, S.K. Seshadri, *Mater. Chem. Phys.*, 99 (2006) 300-308.

23. Y.N. Bekish, S.K. Poznyak, L.S. Tsybul'skaya, T.V. Gaev'skaya, *Electrochim. Acta*, 55 (2010) 2223-2231.
24. A. Karabulut, M. Durmaz, B. Kilinc, U. Sen, S. Sen, *Acta Phys. Pol.*, A 131 (2017) 147-149.
25. L. Tarkowski, P. Indyka, E. Beltowska-Lehman, *Nucl. Instrum. Methods Phys. Res., Sect. B*, 284 (2012) 40-43.
26. Y. Liang, X. Sun, A.M. Asiri, Y. He, *Nanotechnology*, 27 (2016) 12LT01.
27. Z. Liu, Y. Li, X. Huang, J. Zuo, Z. Qin, C. Xu, *Catal. Commun.*, 85 (2016) 17-21.
28. F. Madah, A.A. Amadeh, C. Dehghanian, *J. Alloys Compd.*, 658 (2016) 272-279.
29. R. A. Shakoor, U.S. Waware, R. Kahraman, A. Popelka, M.M. Yusuf, *Int. J. Electrochem. Sci.*, 12 (2017) 4384-4391.
30. B. Li, W.W. Zhang, *Int. J. Electrochem. Sci.*, 12 (2017) 7017-7030.
31. A. Laszczyńska, J. Winiarski, B. Szczygieł, I. Szczygieł, *Appl. Surf. Sci.*, 369 (2016) 224-231.
32. V. Niksefat, M. Ghorbani, *J. Alloys Compd.*, 633 (2015) 127-136.
33. Y. Wang, S. Wang, X. Shu, W. Gao, W. Lu, B. Yan, *J. Alloys Compd.*, 617 (2014) 472-478.
34. E. Beltowska-Lehman, P. Indyka, A. Bigos, M. Kot, L. Tarkowski, *Surf. Coat. Technol.*, 211 (2012) 62-66.
35. K.H. Hou, T.W. Han, H.H. Sheu, M.D. Ger, *Appl. Surf. Sci.*, 308 (2014) 372-379.
36. L. Elias, A. Chitharanjan Hegde, *Surf. Coat. Technol.*, 283 (2015) 61-69.
37. R.A. Shakoor, R. Kahraman, U. Waware, Y. Wang, W. Gao, *Mater. Des.*, 64 (2014) 127-135.
38. S. Dehgahi, R. Amini, M. Alizadeh, *J. Alloys Compd.*, 692 (2017) 622-628.
39. H. Ogihara, M. Safuan, T. Saji, *Surf. Coat. Technol.*, 212 (2012) 180-184

© 2018 The Authors. Published by ESG (www.electrochemsci.org). This article is an open access article distributed under the terms and conditions of the Creative Commons Attribution license (<http://creativecommons.org/licenses/by/4.0/>).